IOP Publishing | International Atomic Energy Agency Nuclear Fusion

Nucl. Fusion **56** (2016) 036013 (15pp) doi:10.1088/0029-5515/56/3/036013

Alpha heating and isotopic mass effects in JET plasmas with sawteeth

R.V. Budny[1] **and JET contributors**[2]

EUROfusion Consortium, JET, Culham Science Centre, Abingdon, OX14 3DB, UK
[1] Princeton University, Princeton, NJ 08540, USA

E-mail: budny@princeton.edu

Received 25 August 2015, revised 6 January 2016
Accepted for publication 12 January 2016
Published 9 February 2016

Abstract

The alpha heating experiment in the Joint European Torus (JET) 1997 DTE1 campaign is re-examined. Several effects correlated with tritium content and thermal hydrogenic isotopic mass $< A >$ weaken the conclusion that alpha heating was clearly observed. These effects delayed the occurrence of significant sawtooth crashes allowing the electron and ion temperatures T_e and T_i to achieve higher values. Under otherwise equal circumstances T_e and T_i were typically higher for discharges with higher $< A >$, and significant scaling of T_i, T_e, and total stored energy with $< A >$ were observed. The higher T_i led to increased ion–electron heating rates with magnitudes comparable to those computed for alpha electron heating. Rates of other heating/loss processes also had comparable magnitudes. Simulations of T_e assuming the observed scaling of T_i are qualitatively consistent with the measured profiles, without invoking alpha heating

Keywords: JET, alpha heating, transport modeling, energy balance, ITER, integrated modeling

(Some figures may appear in colour only in the online journal)

1. Introduction

Alpha heating is essential for practical energy production from deuterium–tritium (DT) fusion reactions. Experiments to detect alpha heating were performed in the tokamak fusion test reactor (TFTR) in 1994 [1, 2] and in the Joint European Torus (JET) in 1997 [3, 4]. The TFTR results were claimed to be consistent with alpha particle heating of electrons. The JET results were claimed to show that alpha particle heating had been unambiguously observed. Measurements of alpha heating were difficult since the alpha heating power profiles p_α were computed to have had magnitudes comparable to some of the other heating and loss rates, and since the experiments were not accurately reproducible. For example, it was difficult to realize comparable deuterium–deuterium (DD), deuterium–tritium (DT), and tritium–tritium (TT) discharges for comparison. One cause of irreproducibility in the JET discharges resulted from the discharges being magnetohydrodynamical (MHD) unstable, which made the flat top phases brief and chaotic. Even before the flat top the presence of sawteeth had large effects. Although significant increases in the electron temperature T_e were observed, and alpha-electron heating $p_{\alpha e}$ most likely was occurring to some extent, the research reported here shows that isotopic mass scaling was clearly observed, and that the alpha heating was not clearly demonstrated.

This paper re-analyzes the discharges used in [3, 4]. These were Hot-ion H-modes with $I_p = 3.8$ MA, $B_{tor} = 3.6$ T, and line-averaged electron density 35% of the Greenwald empirical limit $n_{Gw} = I_p/(\pi a^2)$ [MA m^{-2}]. Edge localized modes (ELMs) occurred late in the neutral beam injection (NBI) phase. The mix of D and T was varied from discharge to discharge by changing the gas inputs and the D and T in the NBI while maintaining their total powers approximately constant ($P_{NB} \simeq 10.3$MW). Several of these discharges had global fusion power gain Q_{DT} (the ratio of fusion power and external heating p_{ext}) of 0.7, and core values q_{DT} (defined in [5]) above 1.1. These are near the highest values achieved in JET.

The fraction of T beam power to total beam power $f_{NBT} = P_{TNB}/P_{NB}$ is an important metric for the scan. Summary values of the discharges are in table 1. Two discharges with

[2] See the appendix of [18].

Table 1. Hot-ion H-mode alpha heating discharges with similar P_{NB}, I_p, and B_{tor}.

Discharge	f_{NBT}	f_{RcT}	δ_t [s]	$< A >$ (14.0s)	$p_{\alpha e}(0)$ [10^{-2}MW m^{-3}]	$n_\alpha(0)$ [10^{17} m^{-3}]	Exceptions
40365	0.0	0.0	0.9026	1.99	0.0	0.0	a,b
41069	0.0	0.0	1.0492	1.98	0.0	0.0	a,b,c
42870	0.27	0.26	0.9515	2.24	2.1	0.38	
42856	0.52	0.68	1.4565	2.55	5.5	1.02	
42855	0.53	0.60	1.2515	2.56	4.5	0.95	d
42847	0.88	0.71	1.4015	2.49	4.0	0.98	e,f
42840	1.00	0.86	1.6100	2.77	2.5	0.60	
43011	1.00	0.98	1.6217	2.92	0.7	0.20	b,g,h

Notes: T beam fraction f_{NBT}; T recycling fraction f_{RcT}; time delay to 1st significant crash δ_t ; core (volume-averaged to $x = 0.2$) hydrogenic mass; alpha electron heating $p_{\alpha e}$; and number of fast alpha ions before the 1st significant crash. Exceptions: a = low I_p; b = low core toroidal rotation; c = low P_{NB}; d = NBI ended early (14.0 s); e = high P_{NB}; f = mode lock disruption; g = high edge n_C; h = high edge recycling.

DD NBI, four with DT, and two with TT are studied here. Six of them were the ones featured in [3, 4]. The additional two are the DD 41069 and the DT 42855. Some exceptional features of these discharges made them more difficult to compare with each other and these are listed in the last column of table 1. Some of these have important implications and are discussed further below. An important parameter is the hydrogenic isotopic mass defined as

$$< A > \equiv (n_H + 2n_D + 3n_T)/(n_H + n_D + n_T), \qquad (1)$$

(using the thermal ion density profiles), which varied from $< A > \simeq$ 2–3 in these discharges. Ranges are shown in table 1.

Profiles of $< A >$ computed for TFTR, shown in [6] are mildly peaked or hollow depending on whether the tritium fueling is dominated by NBI or wall influx. Their core values were used to derive isotopic mass scaling of energy confinement: $\tau_E \propto < A >^{0.7}$. Later studies found $\tau_E \propto < A >^{0.7-0.8}$ [7]. Also, increased ion temperature T_i and reduced thermal ion energy transport χ_i with increasing $< A >$ were observed. This complicated the measurement of the alpha-electron heating p_α since T_i was larger than the electron temperature T_e (in both the TFTR and JET experiments) leading to electron heating from ion-electron energy transfer.

TT discharges, which have larger $< A >$ and smaller $p_{\alpha e}$ and $p_{\alpha i}$, are pivotal for separating alpha heating from isotopic mass effects. The crucial issue is whether these have higher or lower temperatures compared with DT discharges. Higher temperatures would indicate the presence of favorable isotopic mass scaling. The next section demonstrates that the TT discharge considered on in [3, 4] (43011) is not comparable. The other TT discharge (42840), also discussed in [3, 4], is comparable to the others in the scan, and shows a strong isotopic mass effect.

Several publications [4, 8] discussed possible mechanisms, including fast ion stabilization of turbulence and changes in confinement induced by the presence of alpha particles to explain the fact that T_i was unusually high in the DT discharges despite the prediction that the alpha-ion heating $p_{\alpha i}$ is relatively small (calculated to be $\simeq 20\% \times p_{\alpha e}$). The isotopic mass effect is a simple explanation of this. Several effects of increasing $< A >$ contributed to higher T_e in the core and thus mask the effects of $p_{\alpha e}$. Specifically, they delayed the time to significant sawteeth, decreased ion heat transport thereby increasing T_i, and reduced the electron density n_e in the core.

The organization of this paper is to first present the phenomenology of the discharges in the next section showing that: (1) major 'significant' sawtooth crashes were delayed systematically in proportion to the increasing core isotopic mass; (2) the neutron emission rates decreased abruptly or inflected at the crash times indicating that the alpha production was interrupted; (3) the core stored electron energy increased in time at the same rate for all the discharges except during the sudden drops at crash times, indicating that the core electron heating was the same for all unless the transport increased to compensate for additional heating; (4) the temperature profiles increase in time, but splinter accordingly at the sawtooth crashes; (5) a key result is the scaling of temperatures with isotopic mass.

Section 3 presents the TRANSP analysis starting with a demonstration of the accuracy of the results. Careful modeling of sawtooth effects are used for computing $p_{\alpha e}$. The TRANSP analysis is used to compute electron power balance, and even though the alpha heating is predicted to be significant, several terms with considerable experimental uncertainty contribute at levels comparable to the alpha heating. Thus, the modeling and measurements are not sufficiently accurate to separate them.

Section 4 gives a summary, discussion, and suggestions for future alpha heating and isotopic mass experiments.

2. Phenomenology

2.1. General properties of the discharges

Waveforms for one of the highest performing DT discharges are shown in figure 1. A relatively ELM-free phase started after 12.66 s, and gas puffing, used to stabilize MHD modes stopped at 13.5 s. Most of the discharges had phases of low-n MHD as seen in figure 2. The central T_e stopped increasing after the gas puffing stopped and the low-n MHD, such started. Sawtooth crashes cause rapid drops in the core T_e. Crash times were determined from core electron cyclotron measurements of T_e. Examples are shown in figures 2 and 3. Minor disruptions also cause rapid crashes, but sawtooth crashes have simultaneous rapid increases in T_e outside the mixing radius (past the radius where the safety factor is unity). The pattern of frequent small sawteeth crashes with a reduction in frequency after the start of NBI is typically seen in JET beam-heated discharges. Even larger sawtooth crashes occurring early in the NBI phase did not appear to have significant effects on the

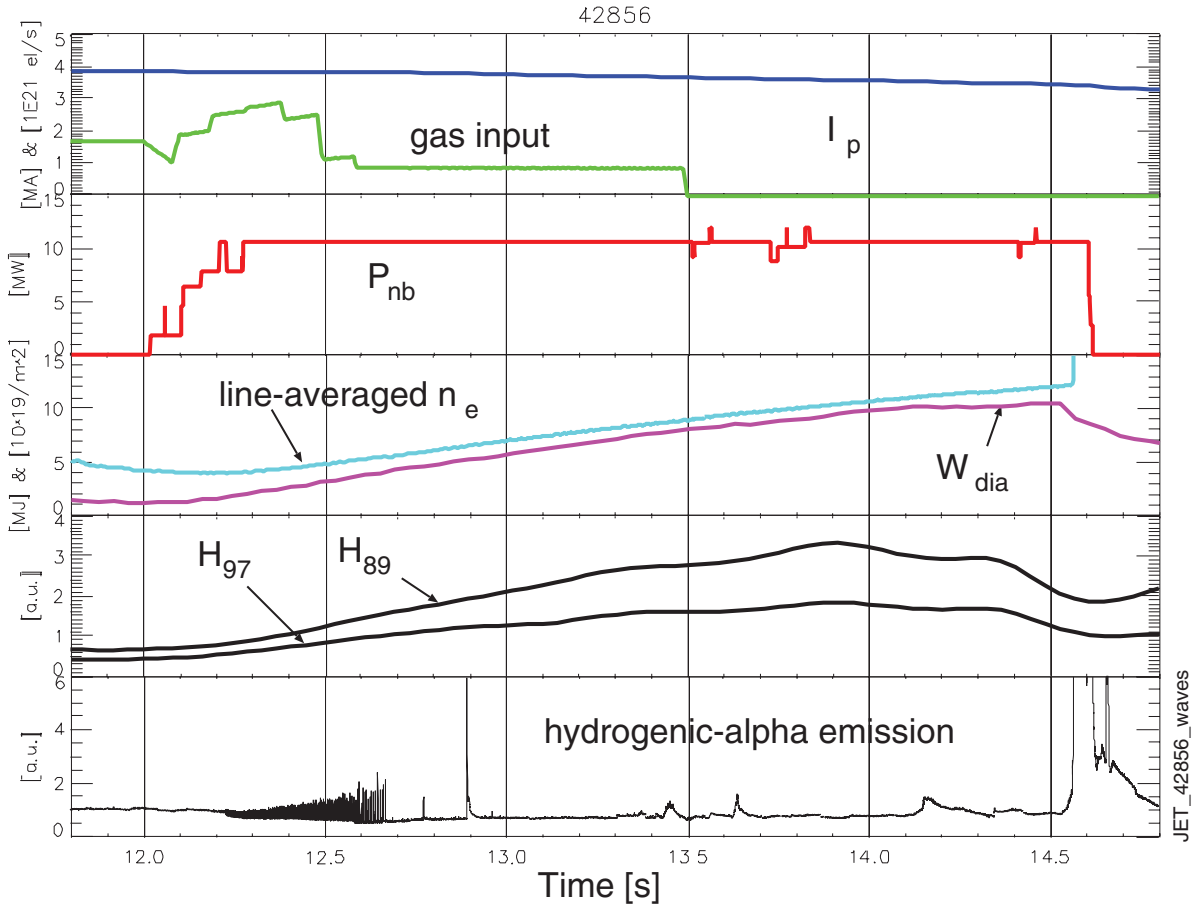

Figure 1. Waveforms for one of the DT discharges showing the plasma current and gas flow; NBI power; line-averaged n_e and stored energy; energy confinement scaling; and the hydrogenic alpha photon emission. A long duration ELM-free phase is seen between 12.66 s and 14.5 s.

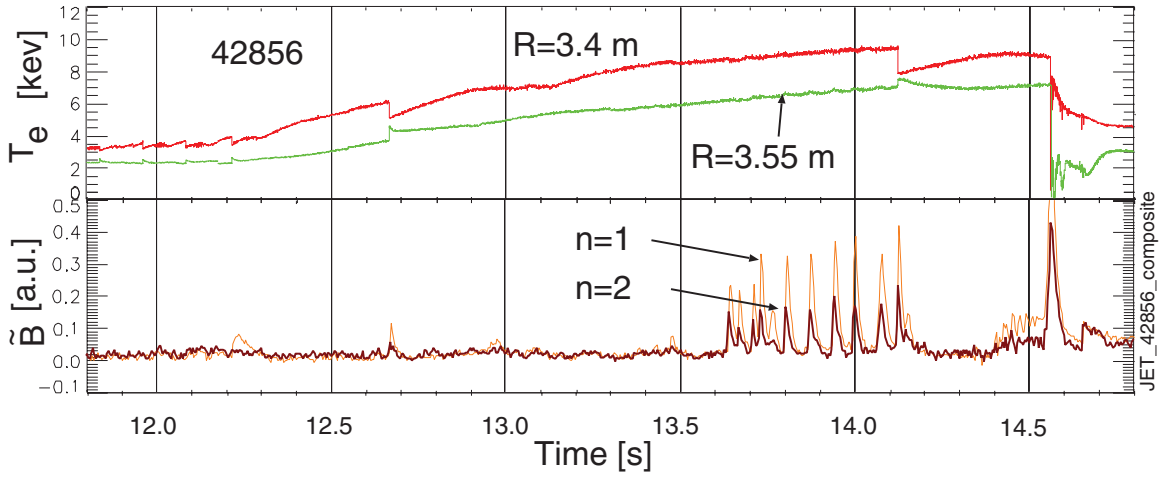

Figure 2. T_e from electron cyclotron emission (ECE) measurements in two channels showing an insignificant sawtooth crash at 12.66 s, a significant crash at 14.13 s; Mirnov coil measurements showing $n = 1$ and 2 MHD modes and a minor disruption with a large increase of n_e at 14.55 s. The peak T_e saturated during the MHD phase.

later performance. However, larger crashes occurring near the end of the stored energy ramp-up and flat top phases did have significant impacts, as discussed below.

Systematic delays in the occurrences of significant sawteeth and giant ELMs with increasing $< A >$ were seen and described in [9], and attributed to longer beam slowing down times and higher beam densities. The analysis described in the next section gives higher core beam densities with increasing $< A >$. Sawtooth crashes were also generally seen in TFTR supershots continuing briefly into the NBI phase with decreasing frequency, but they were generally suppressed later during the NBI phase. Effects of the sawtooth crashes in the JET scan can be seen on the measured total neutron emission rate S_n, and on the central neutron emission rate $s_n(0)$ from fits

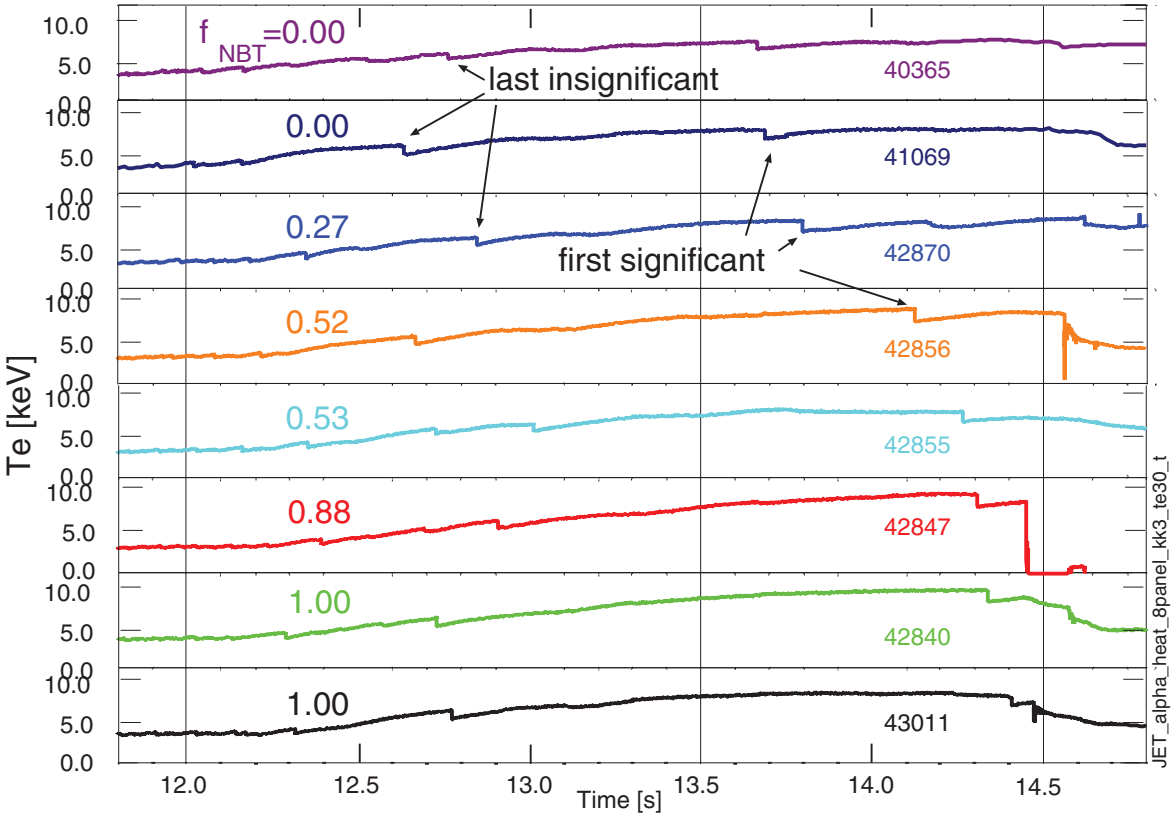

Figure 3. Sawtooth / minor disruption crashes in one of the core ECE signals from the discharges in the alpha heating scan in table 1. Insignificant sawtooth crashes are seen within the first second of NBI which started at 12.0 s. Significant sawtooth crashes and minor disruptions are seen starting after 13.6 s. The times of the first significant sawtooth crashes increased with increasing f_{NBT}.

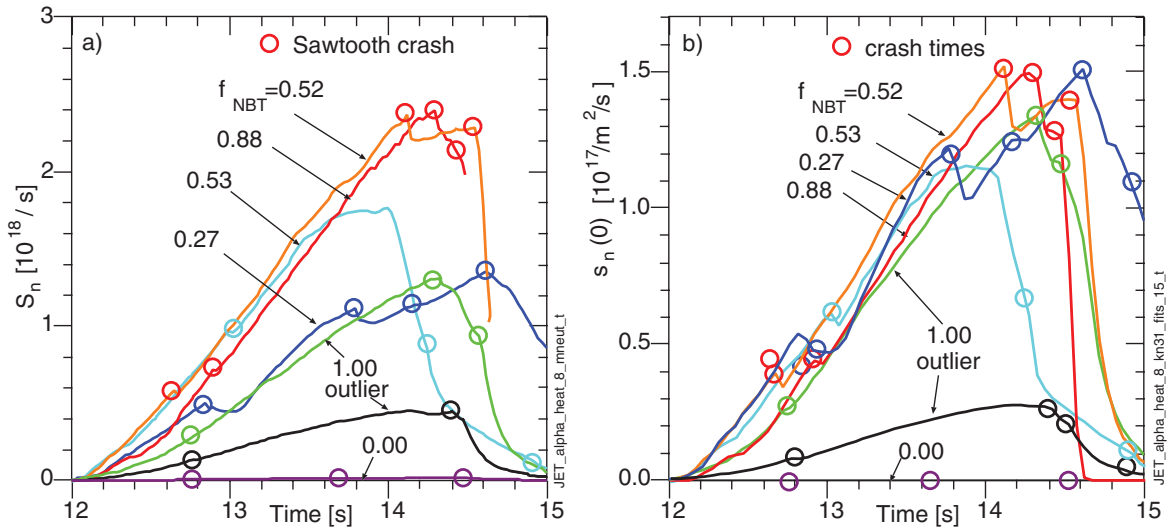

Figure 4. Effects of the sawtooth crashes in the JET scan can be seen on the total neutron emission rate S_{n} and on the central neutron emission rate $s_{\mathrm{n}}(0)$ observed in fits to neutron camera measurements.

to neutron camera measurements shown in figure 4. The drops suggest that beam ion density is mixed, suggesting that alpha heating also drops.

2.2. TT discharges

Pure TT discharges were not achieved in TFTR nor JET due to significant trace amounts of deuterium. A pure TT version of the TT discharge 42840 with $< A > = 3.0$ is predicted by TRANSP to have a peak neutron emission rate of $6.5 \times 10^{16}\,\mathrm{s}^{-1}$ from $T + T \rightarrow \alpha + 2n + 11\,\mathrm{MeV}$ fusion, and peak $p_{\alpha e} = 15\,\mathrm{kW}$. Both the DT and TT fusion reactions have strong contributions from a He^5 spin 3/2 resonance, but the spin and kinematic constraints make the TT rate much lower than the DT rate when the D and T spins are aligned. The DD fusion reaction (at the relevant low center-of-mass energies) has no resonance, and

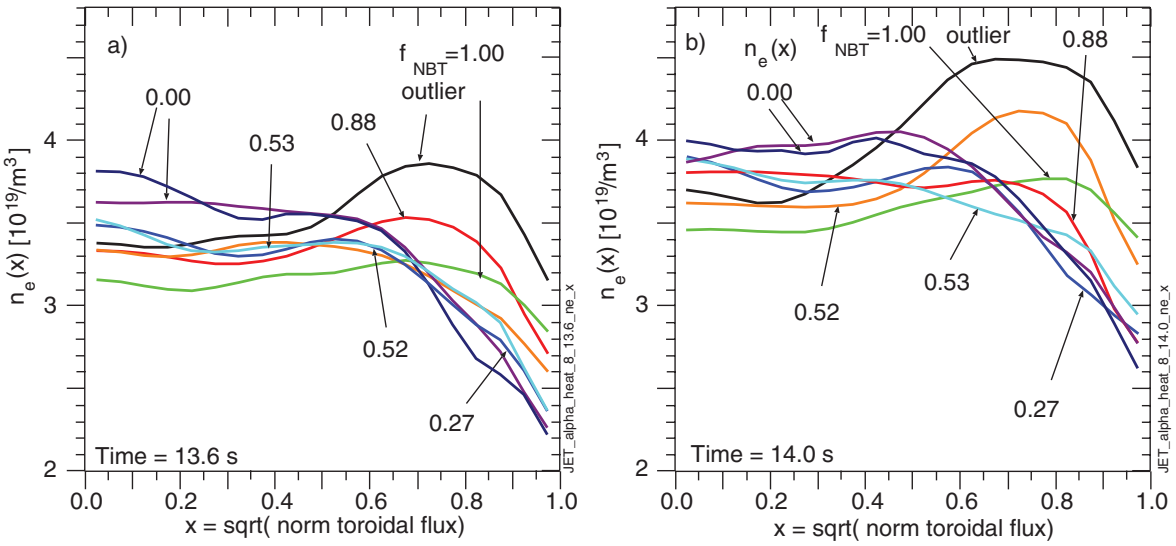

Figure 5. Profiles of n_e at 13.6 and 14.0 s.

approximately four amplitudes contribute with comparable, relatively low magnitudes.

The JET TT discharges in table 1 had measured neutron emission rates S_n equal to 1/4 and 1/2 of the rates from the DT discharges. The one with lower S_n (43011) had T_i and T_e lower than the DT discharges, but it had stored energy nearly the same as the DT 42847, so this pair was considered to be comparable in [3, 4]. This choice was a crucial step for the argument that $< A >$ effects were not playing a significant role, and thus that alpha heating was unambiguously observed. As shown in the next section, this discharge had an exceptionally high recycling rate (50% above any of the others), a higher carbon and edge electron density, and lower T_i and T_e relative to the DT discharges, and to the other TT discharge 42840. Thus, 43011 is not suitably matched with the others.

The TRANSP analysis discussed in section 3 finds that the thermonuclear neutron emission was much lower in 43011 compared with 42840. 43011 is compared with the DT 42847 in figure 1 of [3], and was used to argue that the temperatures roll over in the scan at highest $< A >$. The other TT discharge 42840 had temperatures among the highest of the scan. In this re-analysis this discharge plays a crucial role in establishing the isotopic mass scaling and weakens the role of $p_{\alpha e}$. 42840 is compared with the other discharges in figure 2 of [3] having $n_T/(n_D + n_T) = 0.8$ and $T_e(0) < 11.5$ keV. In the next section the data show it having $T_e(0) > 11.5$ keV. The electron energy confinement time τ_e of this discharge is compared in figure 5 of [3] (with erroneous $n_D/(n_D + n_T) = 0.75$). Radiation emission profiles were not included in the analysis used in Thomas *et al* [3], so τ_e was underestimated. The TRANSP analysis discussed in section 3 gives higher values. The TT discharge 42840 and the DT discharge 42855 are closely matched up to 13.5 s. After this time, the core temperatures in 42855 drooped.

2.3. Alpha heating scan

The n_e profiles were sometimes hollow, as often seen during the JET DT campaign. The typical trend was for the n_e shape to vary from peaked in hydrogen to virtually flat in deuterium and to increasing hollowness in deuterium–tritium and tritium H-mode plasmas [10]. Examples of the n_e profiles are plotted in figure 5 at two times, 13.6 s before any discharges experienced significant sawtooth crashes, and at 14.0 s after both DD discharges did. The measured profile data are mapped by TRANSP (discussed in the next section) versus x(≡ square-root of the normalized toroidal flux).

Carbon density profiles n_C were measured by charge-exchange spectroscopy, shown in figure 6. They peaked at large radii, and were highest for 43011. This peaking contributed to the high peak in n_e near $x = 0.7$. The total hydrogenic ($H_2 + D_2 + T_2$) alpha emission rates measured along a chord are shown in figure 7(a). This correlates with the hydrogenic wall recycling rates. A high recycling rate could also have contributed to the high peaks in n_e near $x = 0.7$ in 43011. This discharge occurred at least 4 weeks after the others in table 1, so wall conditions could have been rather different.

Predictions discussed in section 3 show $p_{\alpha e}$ is concentrated in the core. Since competing heating and loss terms tend to be larger outside the core, the core region is the most interesting here. Despite the variability in the shapes of n_e, the volume-integrated n_e from the magnetic axis to $x = 0.3$, shown in figure 7(b) is nearly the same for the scan. and increased through the beam phase until the late roll over. Since $p_{\alpha e}$ directly affects the stored energy, not necessarily T_e, it is illuminating to focus on the electron and ion energy density profiles w_e and w_i.

In the core, w_e volume-averaged from the magnetic axis to $x = 0.3$ shown in figure 8(a) increased with approximately the same rates from the start of NBI to over 14.0 s except during abrupt decreases at sawtooth crashes. To lowest order, the core w_e is determined primarily by the length of time the NBI was on except for the downshift at significant crashes. Thus, the core appeared to time-integrate the beam heating. Additional heating due to alpha ions in the DT discharges could have been expected to cause higher rates of increase in w_e. The volume-integrated w_i shown in figure 8(b) are less clustered, and started to deviate from a linear increase after 13.0 s.

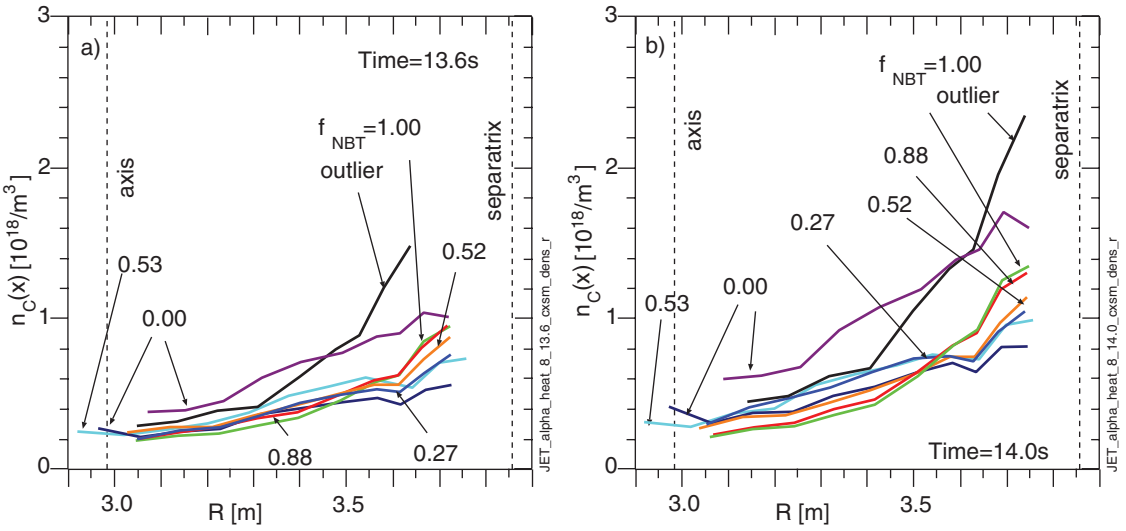

Figure 6. Profiles of n_C at 13.6 and 14.0 s.

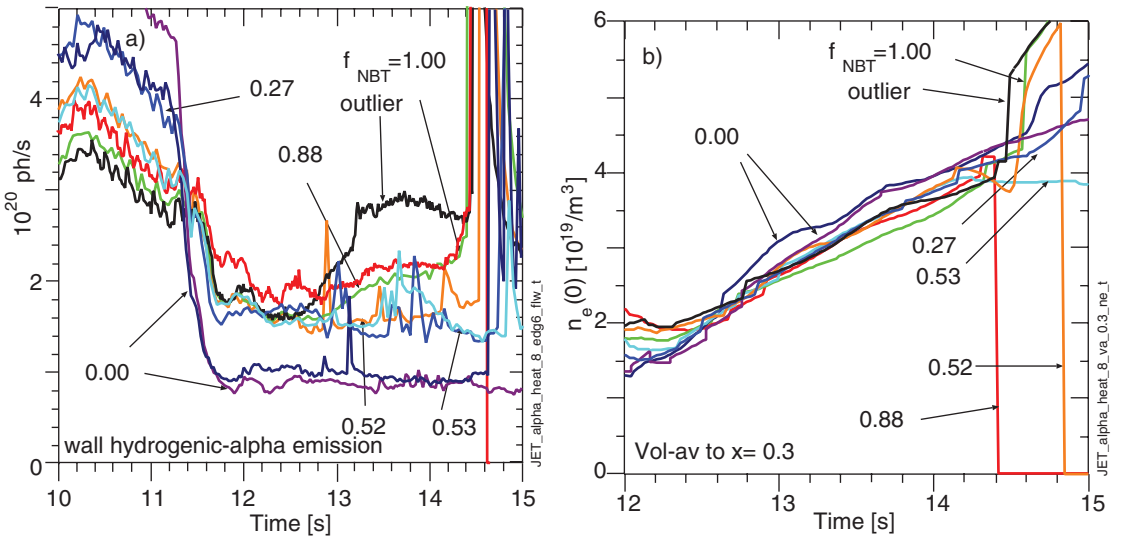

Figure 7. (a) Total hydrogenic alpha photon emission rate; (b) volume-integrals to $x = 0.3$ of n_e.

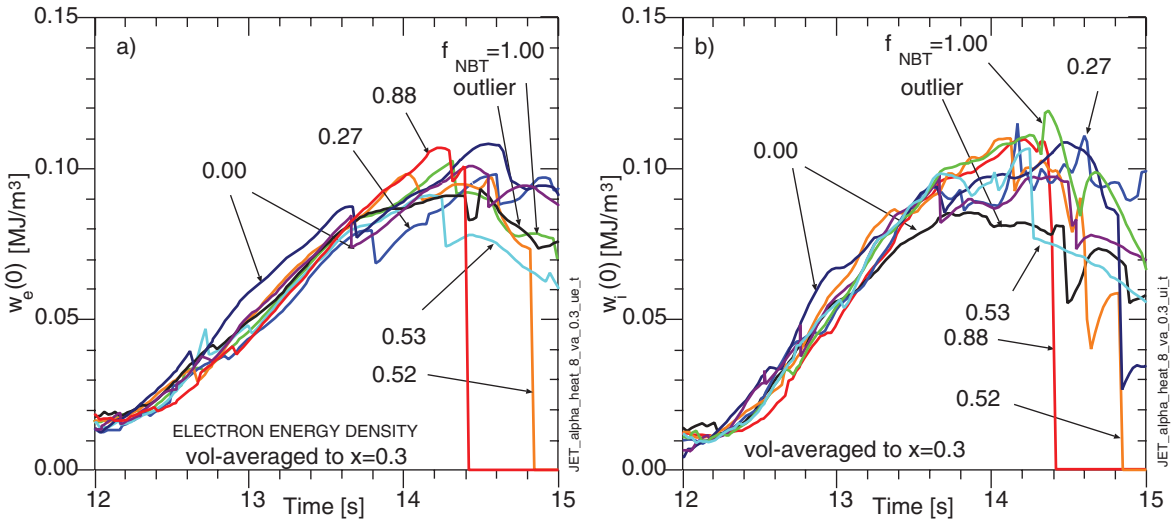

Figure 8. Volume-integrals to $x = 0.3$ of the thermal energy densities (a) w_e, and (b) w_i.

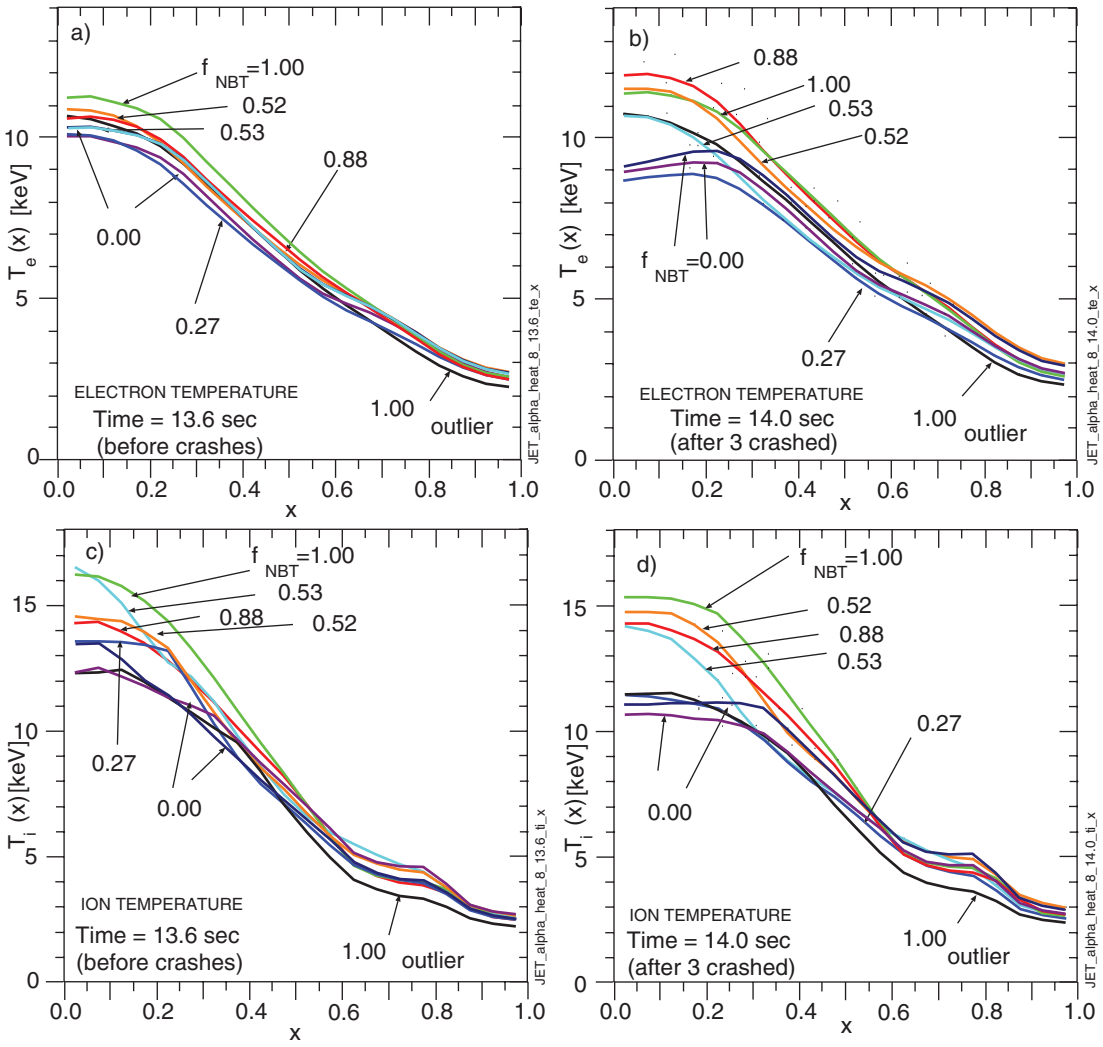

Figure 9. Profiles of (a) $T_e$at 13.6 s (before the first significant sawtooth crash in the scan) and (b) at 14.0s (after the DD discharges and one DT discharge experienced their first significant sawtooth crash); (c) and (d) as above for T_i.

Profiles of T_i for the hydrogenic ions computed by TRANSP from the measured carbon temperature profiles are shown in figures 9(c) and (d) at two times. The carbon-based measurements did not extend beyond $x = 0.8$ so TRANSP used the values at $x = 0.8$ beyond. The profiles have more spread than T_e across the scan. The outlier discharge 43011 with high edge n_e had the lowest edge T_e and T_i, which is expected with high edge n_e and similar heating. The core values of T_e and T_i are also low, which is expected from stiff transport. The other TT discharge 42840 had T_e and T_i among the highest in the scan.

Profiles of T_e are shown in figure 9 at two times: 13.6 s before the first significant sawtooth crash, and 14.0 s after the two DD discharges and one DT discharge crashed. At the later times sawtooth crashes break the tight clustering of rates, and the discharges that have not crashed continue to increase at the same growth rates. By 14 s there is a clear separation of T_e.
An interesting question is whether the temperature gradients were clamped by critical gradients. If so, the critical gradients should be $< A >$ independent according to simple gyrokinetic considerations. These indicate that the critical temperature gradients are independent of mass since they depend on a relationship between the diamagnetic and drift frequencies which have the same mass dependency. Plots of $R/L_{T_e} = -R \times \nabla \ln(T_e)$ and $R/L_{T_i} = -R \times \nabla \ln(T_i)$ are shown in figure 10. High values indicate good confinement. The values in the mid-radius region ($x \simeq 0.3$–0.8) increase roughly 40% as $< A >$ increases across the scan. In this region, $p_{\alpha e}$ is computed to be negligible. In the core the fractional increases with $< A >$ were also large. The data suggests that subtle effects might be in play. For instance, turbulence could be limited by $< A >$ dependant flow shear suppression. The measured toroidal rotation and computed NBI torque profiles had complicated $< A >$ dependencies. Further discussions are given below in the discussion of scalings.

2.4. Isotopic mass scaling

The isotopic mass $< A >$ is calculated from species conservation by TRANSP using the beam-neutral ionization rates and the wall recycling and gas fueling rates. In the core $< A > (0)$ is dominated by the beam-neutral ionization rates, so across the scan $< A > (0) \simeq f_{\rm NBT} + 2$. The time delay δ_t between the last insignificant crash and the first significant crash is another important parameter. Values

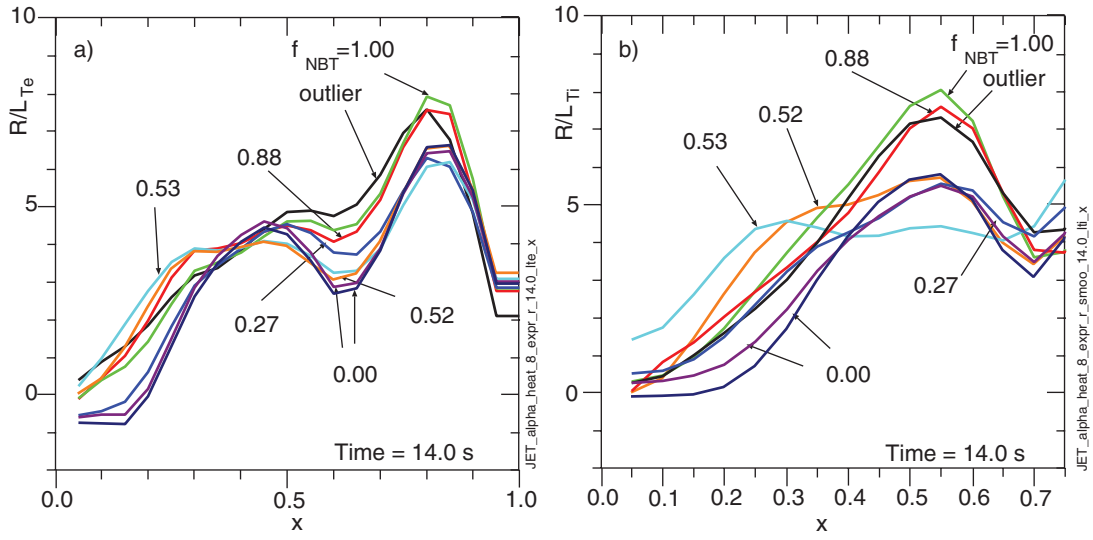

Figure 10. Profiles of (a) $R/L_{Te} = -R \times \nabla \ln(T_e)$ and (b) $R/L_{Ti} = -R \times \nabla \ln(T_i)$ at 14.0 s (after two of the discharges experienced their first significant sawtooth crash).

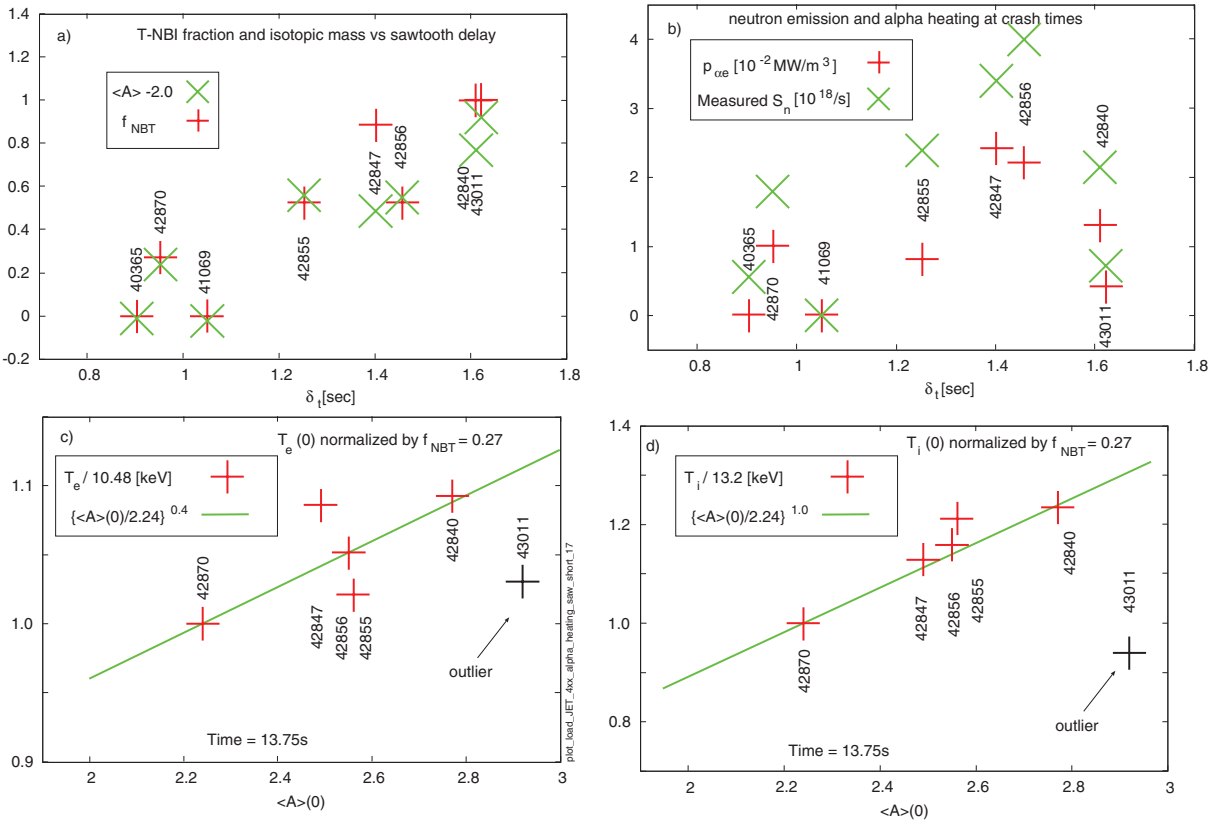

Figure 11. Correlations of delay time δ_t between the last insignificant and the first significant sawtooth crash with (a) isotopic mass and tritium beam power fraction; (b) $p_{\alpha e}$ and S_n at the time of the first significant sawtooth crash; scaling with $<A>$ of (c) core T_i and (d) total stored energy at 13.75 s normalized to values for discharge 42870 (with $f_{NBT} = 0.27$). The DD discharges experienced significant sawtooth crashes by this time and the others did not.

of δ_t in table 1 tend to increase with f_{NBT} and $< A > (0)$ as shown in figure 11(a). Similar correlation is seen using the time of the first significant sawtooth crash instead of δ_t. Neither S_n nor $p_{\alpha e}$ are linearly correlated with δ_t as shown in figures 11(b). This suggests that increasing $< A > (0)$ is the cause of longer δ_t, and thus contributing to the higher core T_i and indirectly T_e.

The trends for T_e and T_i tend to increase with $< A > (0)$, but not so clearly with $p_{\alpha e}$ or S_n which suggests that $p_{\alpha e}$ is not playing a dominant role in T_e, perhaps partly due to systematic changes in confinement or energy loss rates compensating for increased $p_{\alpha e}$. The wider spread of w_i relative to w_e with $< A > (0)$ contributes to the trend of T_e increasing with $< A > (0)$ due to the thermal ion-electron energy coupling p_{ie}.

The scaling in $< A > (0)$ of several variables were deduced at 13.75 s after the DD discharges had significant sawtooth crashes. An advantage of later times is that the discharges are closer to quasi-steady state, and there being more more time for the alphas to slow down, but at later times more discharges experienced significant sawtooth crashes, so there are fewer discharges to compare. The core T_i at 13.6 s scales roughly as $T_i(0) \propto < A >^{0.7}$ if the discharge 43011 is excluded. The scaling at 13.75 s is approximately $T_i(0) \propto < A >^{1.0}$ if 43011 and the DD discharges are excluded. Similarly $T_e(0)$ scales as $\propto < A >^{0.4}$ if 43011 and the DD discharges are excluded. Plots from a database of parameters in the scan are shown in figures 11(c) and (d). Approximate scaling is indicated by the green X's and lines. The stored energy scales roughly as $W_{tot} \propto < A >^{0.3}$ at 13.6 s and as $W_{tot} \propto < A >^{1.0}$ at 13.75. These scalings bracket the scaling of the TFTR supershots.

Scaling of energy transport profiles in JET ELMy H-mode discharge from the DT campaign have been published [10] using local dimensionless parameters: average thermal ion gyro-radius ρ_* and collisionality ν_* normalized by a system scale length, normalized pressure β, and $< A >$. Results for discharges with H, D, or DT in the region $0.3 < x < 0.7$ yielded fits for the ion energy transport $1/\chi_i \propto < A >^{0.84 \pm 0.06}$; the total (convected and conducted) ion energy transport $1/\chi_{itot} \propto < A >^{1.06 \pm 0.06}$; and for the total ion and electron energy transport $1/\chi_{eff} \propto < A >^{0.94 \pm 0.06}$.

Fits using globally-defined (scaler) dimensionless scaling parameters and local $< A >$ taken from the hydrogenic alpha emission (dominated by the edge) are in [11]. The scalings for the thermal energy confinement in ELM-free H modes is $\tau_E \propto < A >^{-0.25 \pm 0.22}$, and in ELMy H modes: $\tau_E \propto < A >^{-0.03 \pm 0.10}$. Local transport analysis of five ELMy H mode plasmas from a dimensionless parameter scaling study of DT plasmas was also presented in [11]. The TT discharge was not well matched, as in this present study. The results gave confinement in the edge region increasing strongly with the isotope mass, whereas the confinement in the core region decreased as $\tau_E \propto < A >^{-0.16}$. In the present study $< A >$ in the core is calculated from species conservation using the NBI and recycling sources using TRANSP, discussed below.

Simple gyrokinetic arguments suggest that the energy transport should have gyro-Bohm scaling, and thus scale in $< A >$ as the sound speed, giving $1/\chi_i \propto < A >^{-0.5}$. This contradicts the results for the alpha heating scan. Often the so-called mixing length is used: $\chi_i \propto \gamma / < k_\perp^2 >$, with γ the mode growth rate and $k_\perp$ the radial wave number. This estimate is based on the assumption that the non-linear saturation is related to the linear drive prescribed by local parameters. Some gyrokinetic simulations have found positive scaling with $< A >$. For instance, a global simulation [12] using Dupree's resonance broadening theory of turbulent wave-particle scattering ($\chi_i \propto \Delta\omega/\Omega_i$) with ω the mode frequency and Ω_i the ion gyro-radius predicts $1/\chi_i \propto < A >^{+0.5}$. Additionally, recent simulations of Ion Temperature Gradient (ITG) and trapped-electron mode (TEM) micro-turbulence [13, 14] indicate that zonal flows have mass-dependent saturation which alters the transport from gyro-Bohm. Another possibility is that flow shear suppression of turbulence had a favorable $< A >$ dependence.

This section argued that the choice in [3, 4] of the dissimilar outlier 43011 for comparison diverted attention from the significance of $< A >$ scaling in the alpha heating discharges. The comparison of T_e in those references at the times just before the last significant sawtooth crash instead of at equal times after the start of the NBI led to an over-emphasis of the increase of T_e in the DT discharges, and to an over-estimation of $p_{\alpha e}$ effects on T_e and consequently of the need for exotic effects to explain high T_i, such as fast ion stabilization of turbulence and changes in confinement induced by the resonance of alpha particles. Here the scaling is attributed to the thermal hydrogenic mass $< A >$.

3. TRANSP analysis, power balance, and simulations

3.1. Model validation

Since the phenomenology does not show clearly the effects of $p_{\alpha e}$, we calculate whether the effects are predicted to be relatively large enough to have been seen. The answer is that $p_{\alpha e}$ is computed to be large, but other contributions with large uncertainties are comparable. The discharges were modeled using the TRANSP code [15] to study heating and transport. Profiles of the temperature, rotation, and density of the trace carbon ions were taken from charge exchange spectroscopy measurements. Measurements of the relative beryllium-to-carbon density ratio from charge-exchange spectroscopy at one radius are available for some of the discharges. The ratio indicates that Be as well as C ions were diluting the deuterium and tritium fuel in the core.

The radiation emission profile p_{rad} is needed for the electron power balance, but is not available, so TRANSP is used to predict the line, bremsstrahlung, and synchrotron emission. Their total volume-integrated rates scale in time approximately as the measured total (core and scrape-off) radiation emission, but are lower by a factor of about 2–3, except two times higher for the outlier 43011. These differences could be caused by the fact that TRANSP computes only the radiation within the separatrix, or that the discharges have significant radiation emission from trace high-Z impurities. The radiation profiles were not scaled to match the total measured due to these uncertainties.

The wall recycling rates are needed to calculate convective transport, neutral ion densities (needed in the calculation of charge-exchange losses), and inflows of H, D, and T. The hydrogenic (H + D + T) alpha emission rates shown in figure 7(a) are scaled to estimate the ionization rate within the boundary (close to the separatrix). The relative amounts of H, D, and T in this total were measured. These rates are systematically low for the DD discharges and high for those with large f_{NBT}. These are used to indicate their partition in TRANSP for the wall source rates in the particle conservation equations.

The modeling achieves approximate agreement with S_n and $s_n(0)$, as well as with the EFIT diamagnetic energy indicating that the modeling is approximately accurate. This is needed to

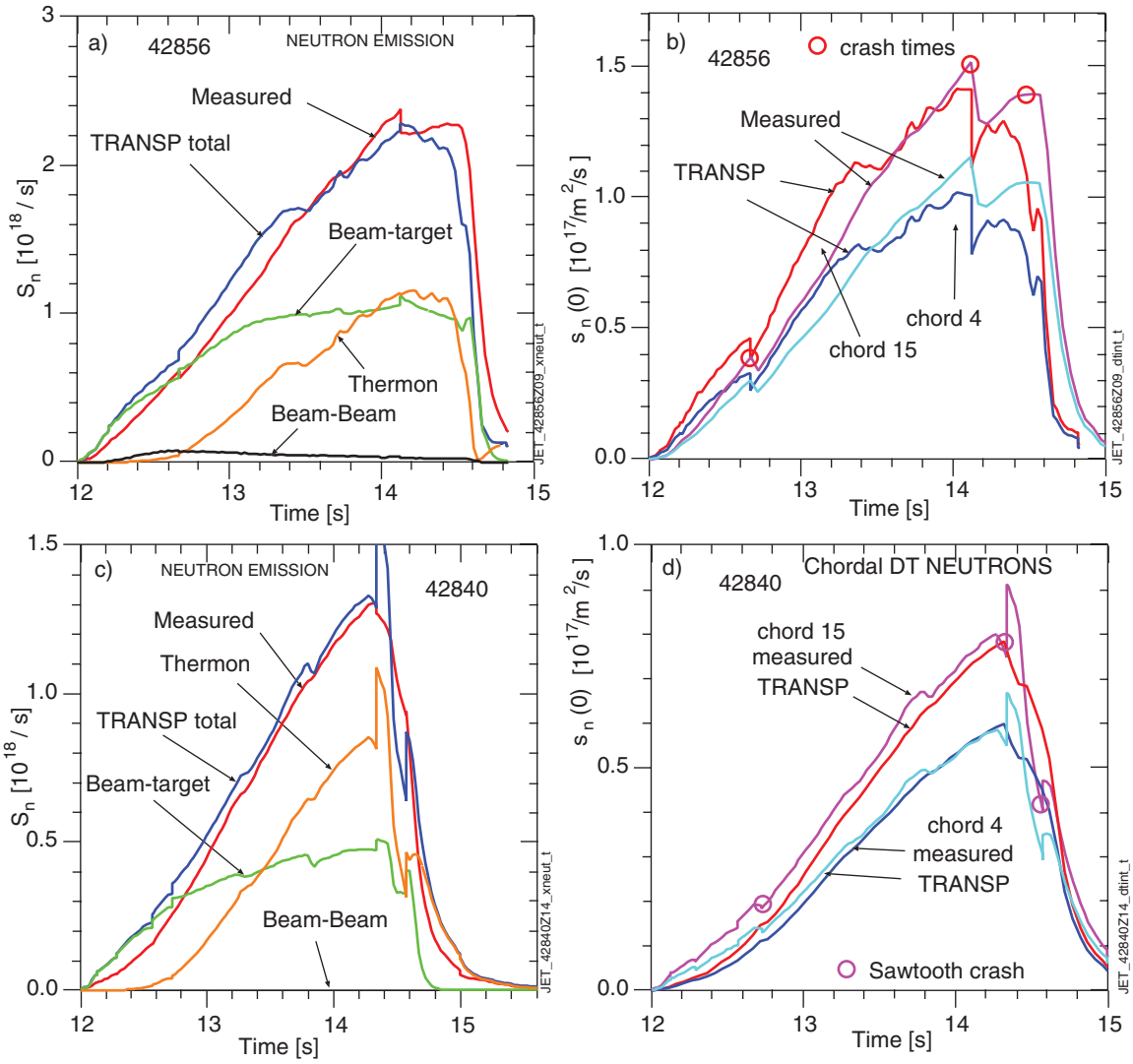

Figure 12. Comparisons for a DT discharge 42856 of simulated and measured (a) global neutron emission rates S_n and (b) local neutron emission rates and $s_n(0)$ which stepped down at the first significant sawtooth crash which occurred at 14.12 s. (c), (d) Similar comparisons for TT discharge 42840.

indicate that the computed $p_{\alpha e}$ is credible. Examples of comparisons for two of the discharges are shown in figure 12. The largest discrepancy between the simulated and measured $s_n(0)$ for the $f_{NBT} > 0$ discharges differ by at most 12% at the peak. The agreements for the $f_{NBT} = 0$ discharges are less accurate. The TT 42840 has good agreement. The fraction of T in the measured hydrogenic recycling f_{RcT}, shown in table 1, was close to the fraction which gave good agreement with $s_n(0)$. The outlier 43011 was problematic in that results using $f_{RcT} \simeq 1.0$ predicted S_n far too low. The best TRANSP simulation is achieved with the recycling tritium fraction set to 80%. One possibility for more accurate predictions of S_n keeping $f_{RcT} \simeq 1.0$ would be to assume a non-zero D component in the NBI.

The sawtooth crashes are modeled assuming Kadomtsev helical mixing of current and fast ions at the sawtooth crash times observed in T_e. The q_{MHD} profiles were not measured, so they were calculated in TRANSP from poloidal field diffusion assuming neoclassical resistivity. In the core, q_{MHD} increased to near unity at the sawtooth crashes.

Sawteeth crashes have been observed to mix fast beam and alpha ions [16]. The TRANSP-predicted helical mixing of the normalized toroidal pressure of the beam β_{bm} and alpha ions β_α is shown in figures 13. The β_{bm} profile recovers in the time scale of the core NBI deposition and the β_α profile recovers in the longer time scale of the core DT fusion rate p_{DT}. The fast alpha density recovers on the time scale of the DT fusion rate and the $p_{\alpha e}$ profile recovers in the time scale of the alpha slowing time, which is $\simeq$1 s, figure 13(d). The core $p_{\alpha e}$, fast alpha density n_α and pressure β_α increase approximately linearly in time, except for sharp crashes at sawtooth crashes as shown in figure 14. TRANSP analysis of sawtooth effects does not appear to have been included in [3], so the values of $p_{\alpha e}$ could have been over-estimated. At 13.6 s the predicted peak core averaged $p_{\alpha e}$ is half the maximum calculated for the scan. In 42856 at 14.1 s the peak predicted ratio $p_{\alpha e}/p_{ext}$ is near 0.2. After 14.55 s, as the density increased following the minor disruption, p_{ext} decreased, and the predicted ratio increased rapidly to a peak of 0.8, but the prediction is very uncertain.

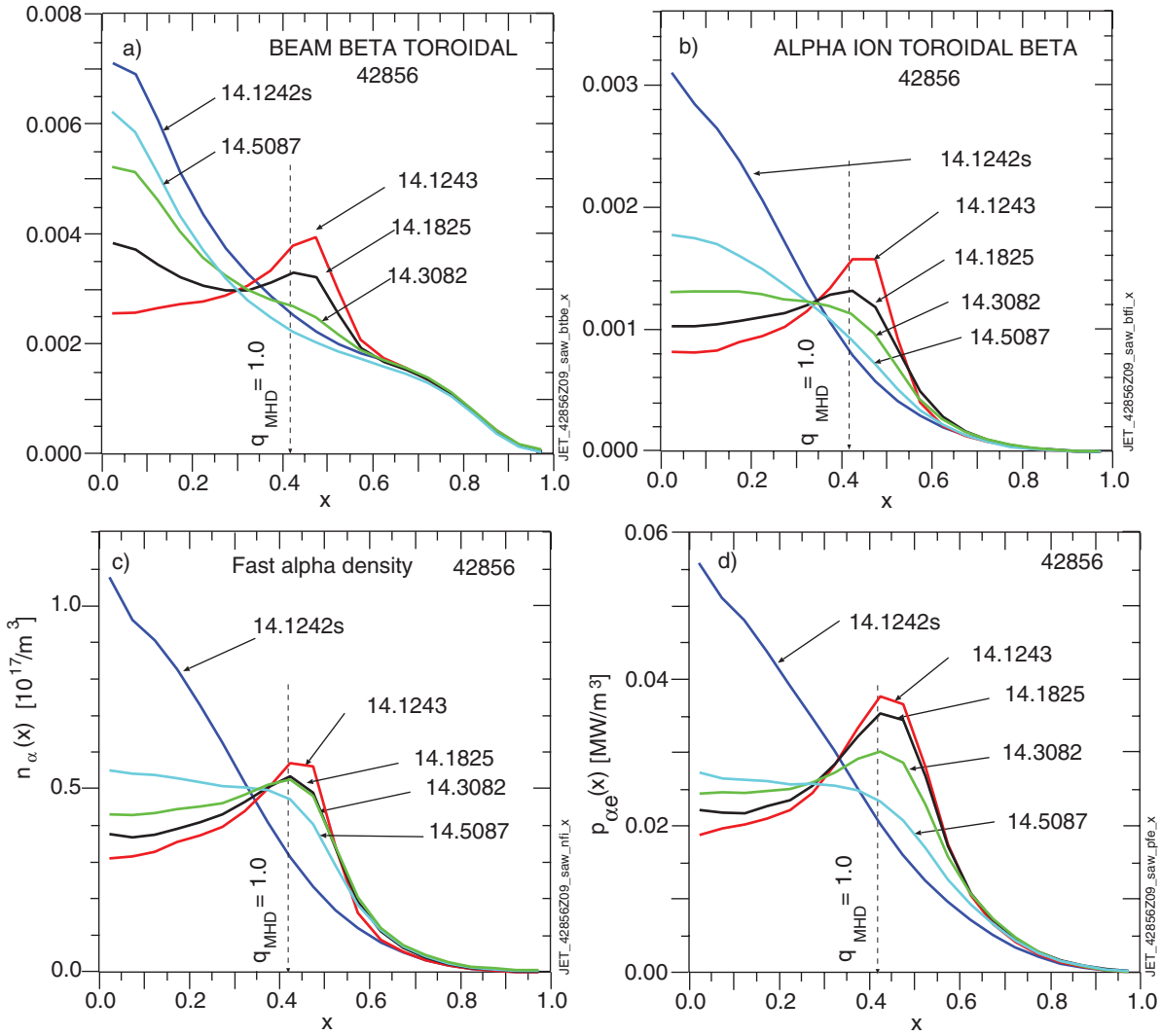

Figure 13. TRANSP predictions of sawtooth mixing effects after the first significant sawtooth crash for the DT discharge with $f_{\mathrm{NBT}} = 0.52$ shown in figure 12 (a) beam and (b) fast alpha normalized ion pressures; (c) alpha density and (d) alpha-electron heating.

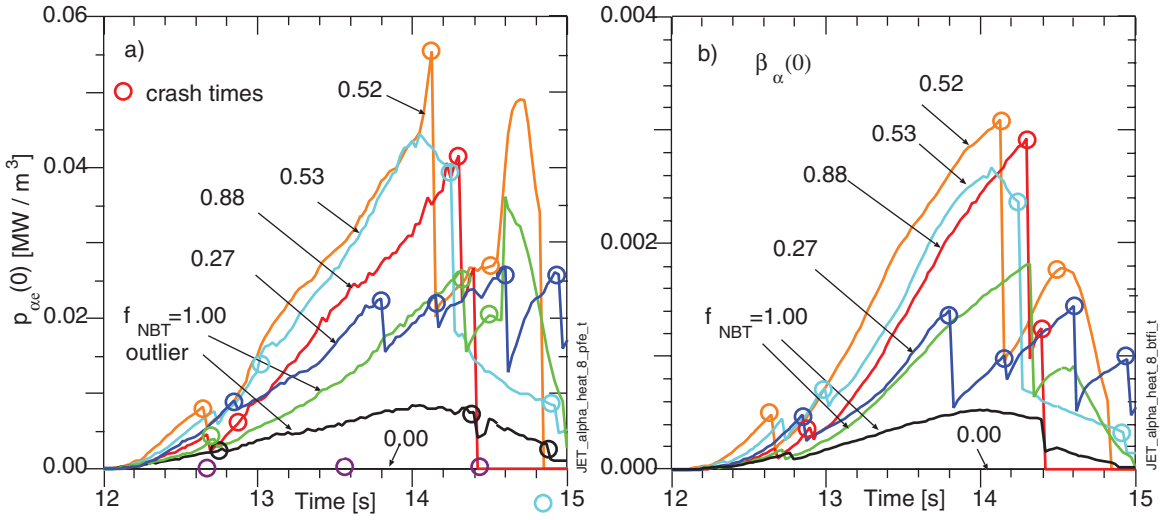

Figure 14. Sawtooth effects on central (a) alpha-electron heating, and (b) normalized alpha pressure. The discharge 52856 with $f_{\mathrm{NBT}} = 0.52$ had a minor disruption after 15.56 s so the alpha heating did not have time to recover from the sawtooth crash.

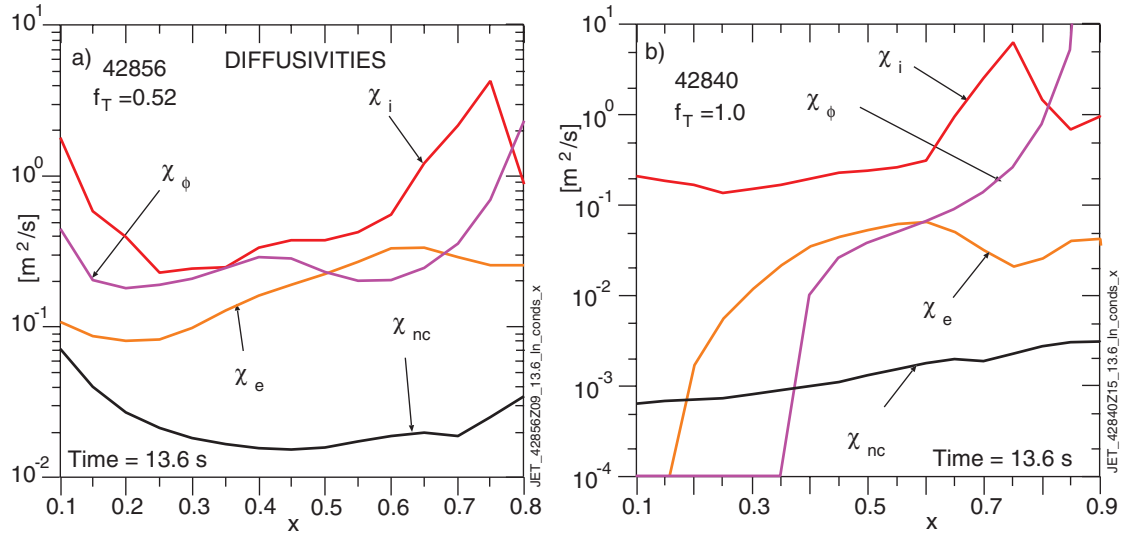

Figure 15. Profiles of transport coefficients for one of the (a) DT and (b) TT discharges.

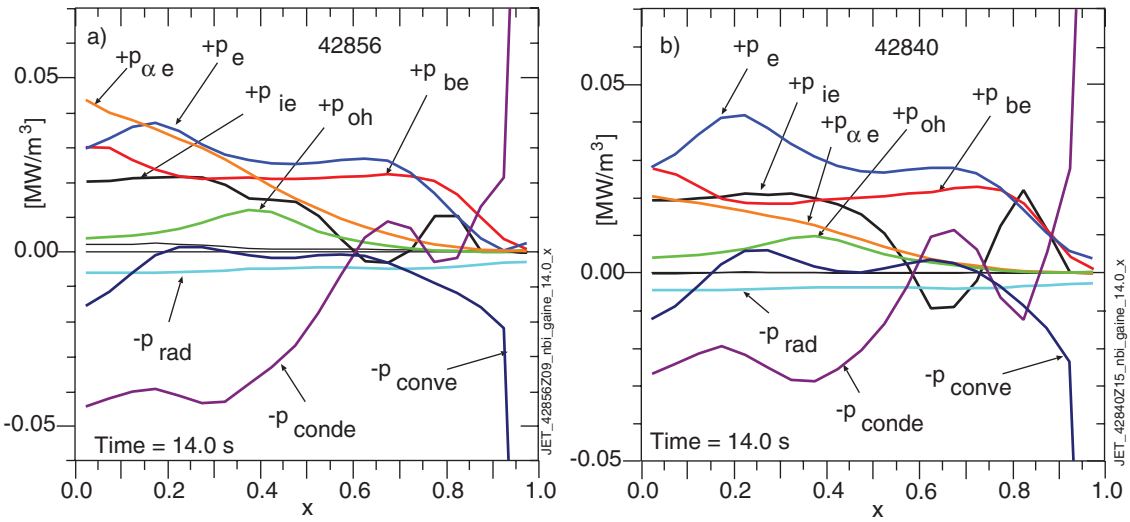

Figure 16. Profiles of the electron heating and loss terms for one of the (a) DT and (b) TT discharges.

3.2. Power balance

TRANSP analysis uses measurements to calculate the heating and loss source rates and the gradients of the power flows. The terms for w_e and w_i are:

$$\frac{\partial w_e}{\partial t} = p_e \equiv p_{be} + p_{\alpha e} + p_{oh} + p_{ie} + p_{cmpe} - p_{rad} - p_{conde} - p_{conve} - p_{ioniz} \quad (2)$$

$$\frac{\partial w_i}{\partial t} = p_i \equiv p_{bi} + p_{cmpi} + p_{rot} + p_{rot} - p_{ie} - p_{cx} - p_{condi} - p_{convi}. \quad (3)$$

The ionization and compression terms p_{ioniz} and p_{cmpe} are negligible in the core. In the usual analysis mode, TRANSP computes the convected and conducted power losses p_{conve} and p_{conde}. Examples of the computed transport coefficients are in figure 15. The electron conduction coefficient χ_e is rather low compared to χ_i. Either larger p_{rad} or lower $p_{\alpha e}$ would reduce χ_e further. Profiles of the heating terms are shown in figure 16.

To study $p_{\alpha e}$, consider the time and volume integrals:

$$\int_0^x dV w_e \simeq w_e(t = 12) + \int_0^x \int_{12}^t dt dV p_e \quad (4)$$

integrated to $x = 0.3$, and time integrated from 12.0 s. The reason for starting time at 12 s is that the simulations are considerably less certain at earlier times before the charge-exchange spectroscopy data window. Profiles at 14.0 s are shown in figures 17(a) and (b), and the time evolutions in figures 17(c) and (d). The dominant term is the beam-ion-electron heating p_{be}. During the end of the ramp-up and into the flat-top phases the terms p_{oh}, p_{ie}, p_{conde}, and $p_{\alpha e}$, and perhaps p_{rad} contribute roughly equally, except for the $f_{NBT} = 0$ discharges where $p_{\alpha e}$ is negligible. The presence of these uncertain terms make it is difficult to accurately quantify $p_{\alpha e}$

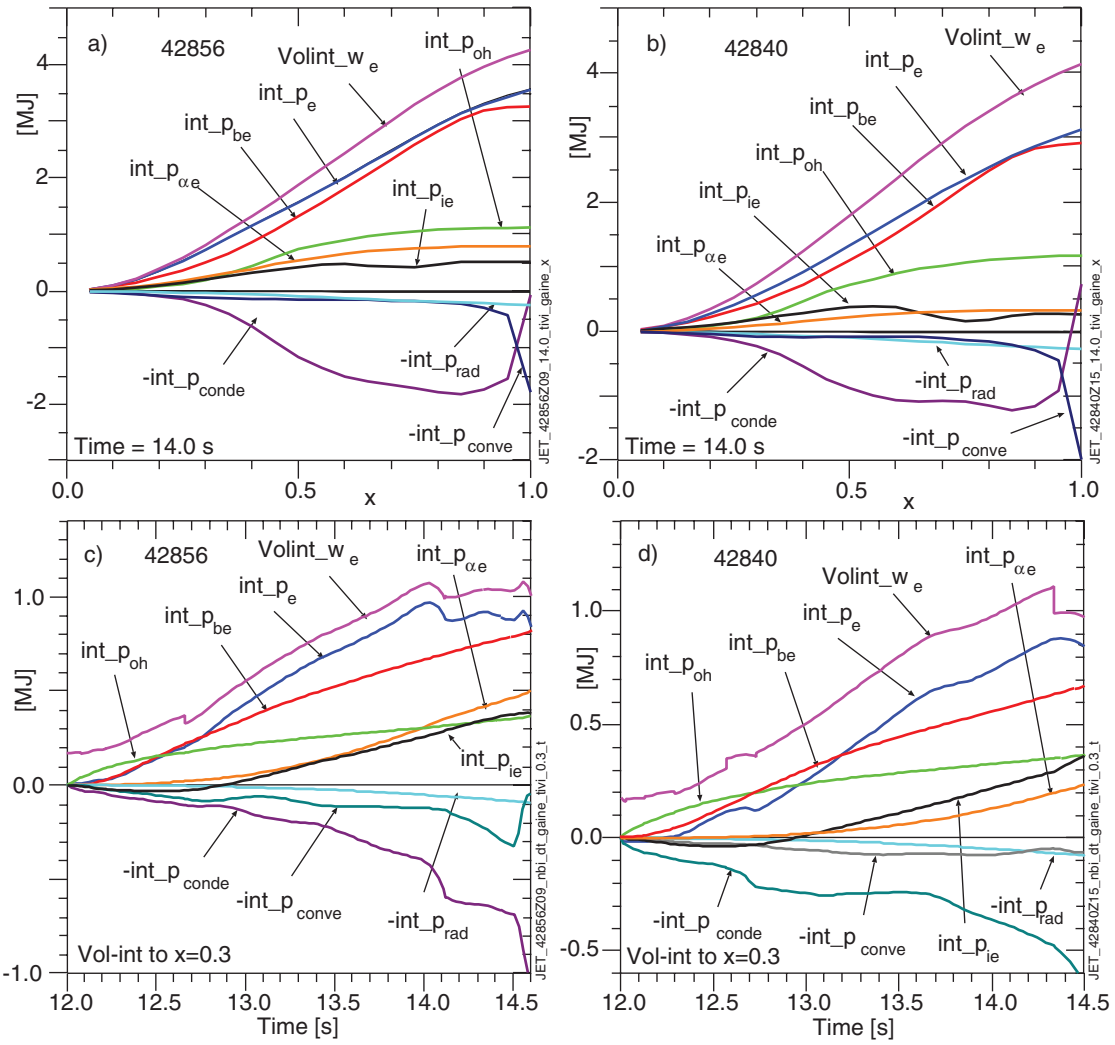

Figure 17. Profiles at 14.0 s of the time- and volume-integrated electron heating p_e and the volume-integrated w_e in the (a) DT and (b) TT discharges; time evolutions of the time- and volume-integrated electron heating p_e and the volume-integrated w_e in the (c) DT and (d) TT discharges.

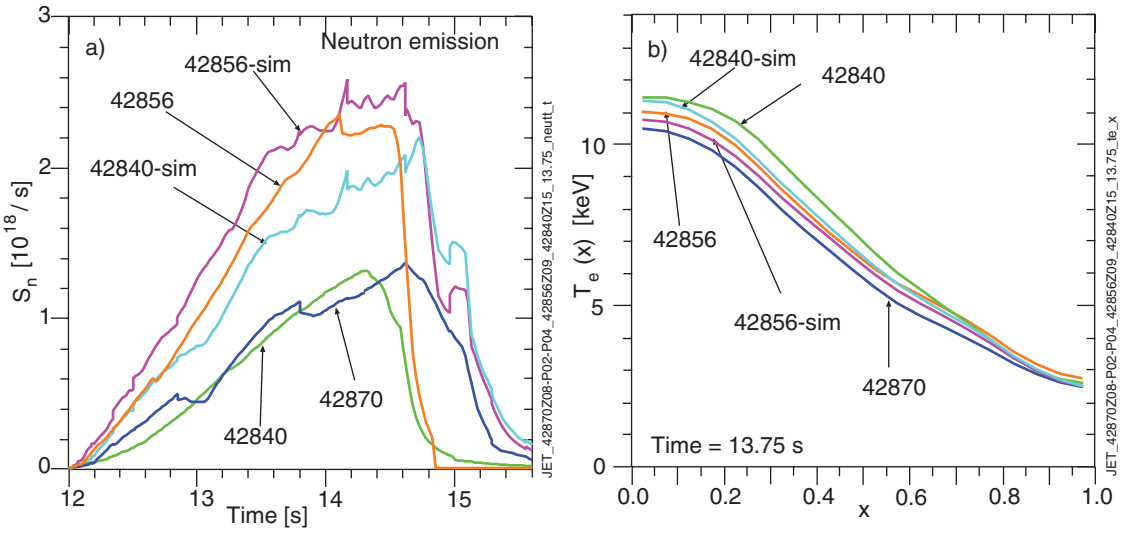

Figure 18. Simulations of 42856 and 42840 denoted sim derived from TRANSP analysis of 42870 assuming $< A >$ scaling of T_i, keeping χ_e fixed, and zero $p_{\alpha e}$. (a) Total neutron emission in the predictions, measured S_n in the analysis runs; (b) predicted T_e and TRANSP mapped measurements in analysis runs.

in the power balance results. The total thermal electron stored energy $\int \mathrm{d}Vw_\mathrm{e}$ increased at a rate of about 2 MW.

A similar analysis of the ion power balance (equation (3)) is further complicated by the scarceness of the charge-exchange data. One large uncertainty is the charge-exchange loss term p_cx which is estimated (from the estimated recycling rate). The volume integrated electron energy $\int_0^1 \mathrm{d}Vw_\mathrm{i}$ increased at a constant rate $\simeq$2 MW early in the NBI phase, then rolled over by 1.5 s.

3.3. Simulations of T_e without alpha heating

Even if the experiments are consistent with alpha heating, the inverse should be checked: are they consistent without alpha heating? To what extent could the $< A >$ scaling of T_i replace the role of $p_{\alpha e}$ in increasing T_e? TRANSP was used to predict discharges like 42856 with $f_\mathrm{NBT} = 0.52$ and 42840 with $f_\mathrm{NBT} = 1.0$ assuming $< A >$ scaling of $T_\mathrm{i} \propto < A >^1$ but without alpha heating. The analysis run for the discharge 42870 with $f_\mathrm{NBT} = 0.27$ was used with 42840 with $f_\mathrm{NBT} = 1.0$ if the T_i input were scaled up by their ratios of $< A >$ in table 1, and χ_e were held fixed. The predictions do not take into account the differences in n_e in these discharges. These results for the simulated S_n and T_e are shown in figure 18. The T_e profiles are in qualitative agreement with figure 9(a). Both simulations have p_ie nearly double the analysis values.

4. Summary, discussion, and conclusions

Re-analysis of the alpha heating experiments in the JET 1997 DTE1 campaign results in significant differences with the previous published analysis [3, 4]. The TT discharge used in those papers to conclude the absence of isotopic mass effects is found to be unsuited for inclusion in the scan, due to its high recycling rate. The re-analysis using the other, more comparable TT discharge in the scan shows that at equal times in the discharges, core T_i, T_e, and the total stored energies scale approximate linearly with the average thermal hydrogenic ion mass $< A >$. The core $< A >$ is strongly correlated with the increase of the sawtooth delay δ_t, and the delays of significant sawtooth crashes allowed T_e and T_i to obtain higher values. Thus, longer δ_t and p_ie could explain the higher T_e. The computed $p_{\alpha e}/p_\mathrm{ext}$ is up to 0.2, but electron power balance in the core shows that multiple terms with relatively large uncertainties are comparable to the computed $p_{\alpha e}$. Another difference with the previous analysis is that the inclusion of sawtooth effects results in lower values for the computed $p_{\alpha e}$.

The initial studies [2] of alpha heating in TFTR showed significantly higher core T_e in DT supershots compared with DD and TT supershots. The beam and thermal core electron heating was argued to be independent of P_DT, and the rise of computed P_α heating with P_DT was correlated with increased $T_\mathrm{e}(0)/\tau_\mathrm{E}^{0.5}$. A re-analysis of electron heating in the TFTR alpha heating discharges similar to the results reported here has not been conducted. An example of a similar electron power balance analysis for a TFTR supershot is shown in [5]. The discharge studied there (the supershot with highest Q_DT) had very high $T_\mathrm{i}/T_\mathrm{e}$ and thus high p_ie at the time of maximum P_DT. The ratio of the computed $p_{\alpha e}$ and p_ext in the core is 0.05, to be compared with 0.20 for the JET 42856. The corresponding ratio computed for the JET Hot-ion H-mode discharge with highest Q_DT is 0.12 [5]. In the TFTR supershot, late, after a minor disruption and impurity influx, the ratio is computed to be 0.8, as was the case for the JET 42856 after it experienced a minor disruption, but the measurement and analysis uncertainties are large. Large increases in the central T_e were often observed in TFTR following the termination of NBI.

Various aspects of the analysis and modeling need further study to increase confidence in the simulations. Examples are the alpha heating $p_{\alpha e}$ and $p_{\alpha i}$ and loss terms, for instance the effects of MHD. Additionally, the sawtooth model in TRANSP is simplistic and the sawtooth mixing predictions for alpha ions would benefit from further testing.

Future DT experiments are planned for JET in 2018 and the international thermonuclear experimental reactor (ITER) in 2034. Alpha heating and isotopic mass experiments in JET would benefit from a more comparable set of discharges, especially including ones with TT NBI. Avoiding sawteeth could improve the reproducibility and simplify the modeling. Measurements such as radiation, recycling, and impurity densities would improve the analysis. Separating alpha heating effects from isotopic mass effects are important, especially since isotopic mass enhancements of transport could help make DT fusion energy possible.

One question concerning the extrapolation of isotopic mass effects to ITER is to what extent do these effects depend on the fast ion density and energy. The fast ion density fractions in TFTR supershots and JET Hot-ion H-mode discharges were higher than anticipated in ITER. Another question is whether the mass scaling depends on a high ratio $T_\mathrm{i}/T_\mathrm{e}$. This ratio was relatively high in the TFTR supershots and JET Hot-ion H-mode discharges. Also the toroidal rotation Mach number predicted for ITER is low [17] relative to values seen in high performance TFTR and JET discharges. Thus rotation-induced flow shear could be less favorable in ITER.

Acknowledgments

This work has been carried out within the framework of the EUROfusion Consortium, and has received funding from the Euratom research and training programme 2014-2018 under grant agreement No 633053. The views and opinions expressed herein do not necessarily reflect those of the European Commission. This work was also supported in part by the US DoE contract No. DE-ACO2-76-CHO3073. The author wishes to thank D. Campbell, S. Zweben, and two referees for very helpful comments.

References

[1] Hawryluk R.J. *et al* 1994 *Phys. Rev. Lett.* **72** 3530
[2] Taylor G., Strachan J.D., Budny R.V. and Ernst D.R. 1996 *Phys. Rev. Lett.* **76** 2722

[3] Thomas P.R. *et al* 1998 *Phys. Rev. Lett.* **80** 5548
[4] Sharapov S.E. *et al* 2008 *Fusion Sci. Technol.* **53** 989
[5] Budny R.V. and Cordey J.G. 2016 Core fusion power gain and alpha heating in JET, TFTR, and ITER *Nucl. Fusion* submitted
[6] Budny R.V. *et al* 1994 *21st EPS Conf. on Controlled Fusion and Plasma Physics (Montpelier, France, 27 June–1 July 1994)* available at http:w3.pppl.gov/ budny/PDF/Budny_EuropeanPhysicalSociety_1994.pdf
[7] Scott S.D. *et al* 1995 *Phys. Scr.* **51** 394
[8] Testa D. and Albergante M. 2012 *Nucl. Fusion* **52** 083010
[9] Nave M.F.F. *et al* 2001 *Nucl. Fusion* **42** 281
[10] Budny R.V. *et al* 2000 *Phys. Plasmas* **7** 5038
[11] Cordey J.G. *et al* 1999 *Nucl. Fusion* **39** 301
[12] Lee W.W. and Santoro R.A. 1997 *Phys. Plasmas* **4** 169
[13] Hahm T.S., Wang L., Wang W.X., Yoon E.S. and Duthoit F.X. 2013 *Nucl. Fusion* **53** 072002
[14] Bustos A., Banon Navarro A., Gorler T., Jenko F. and Hidalgo C. 2015 *Phys. Plasmas* **22** 012305
[15] Budny R. 1994 *Nucl. Fusion* **34** 1247–62
[16] McKee G. *et al* 1995 *Phys. Rev. Lett.* **75** 649
[17] Budny R.V. 2009 *Nucl. Fusion* **49** 085008
[18] Romanelli F. *et al* 2014 *Proc. of the 25th IAEA Fusion Energy Conf. (Saint Petersburg, Russia, 2014)*